MINISTRY OF EDUCATION AND TRAINING

VIETNAM ACADEMY OF SCIENCE AND TECHNOLOGY

GRADUATE UNIVERSITY SCIENCE AND TECHNOLOGY

NGUYEN THI HAI YEN

MOTT TRANSITION AND ANDERSON LOCALIZATION IN SOME STRONG CORRELATED FERMION SYSTEMS WITH DISORDER

Major: Theoretical and Mathematical Physics
Code: 9.44.01.03

SUMMARY OF DOCTORAL THESIS

SUPERVISOR: ASOCI. PROF. HOANG ANH TUAN

Ha Noi - 2024

The dissertation is completed at: Graduate University of Science and Technology, Vietnam Academy Science and Technology

Supervisors:

1. Supervisor 1: Assoc. Prof. Dr. Hoang Anh Tuan

Referee 1:.....

Referee 2:.....

Referee 3:.....

The dissertation will be examined by Examination Board of Graduate University of Science and Technology, Vietnam Academy of Science and Technology at…….. (time, date……)

The dissertation can be found at:

1. Graduate University of Science and Technology Library
2. National Library of Vietnam

INTRODUCTION

Motivation

The correlated and disordered lattice fermion systems have been at the forefront of condensed matter research for decades. In particular, Coulomb interaction prevailing in strongly correlated electron systems and disorder are two main sources leading to metal - insulator transitions (MITs). While the correlation induced MITs are called Mott- Hubbard transition, the coherent backscattering of non-interacting particles from randomly distributed impurities can cause Anderson localization. Thus, it can be said that the interplay between disorder and interaction leads to many interesting effects and poses fundamental challenges for both theory and experiment in physics. In the field of ultracold atoms in optical lattice, where the parameters of the system are easily controlled and changed. Then, we will study the same problems in more complex and real models, such as the mass-imbalanced Anderson – Hubbard model.

Objectives

The aim of this project is to study Anderson localization and the Mott-Insulator in some disordered and interacting fermion systems on two models AFKM and AHM.

Contents

1) Investigate the influence of the Gaussian distribution of disorder on the phase diagram for the AHM and AFKM models. 2) Study the phase diagram of the asymmetric AHM model at half-filling and the AHM model with a site-dependent interactions.

Chapter 1

MOTT INSULATOR, ANDERSON INSULATOR, TYPICAL MEDIUM THEORY, AND OPTICAL LATTICE

1.1 Mott Insulator and Anderson Insulator

1.1.1 Mott insulator

In solid state physis, one can be distinguish the materials to the conductors, insulators and semiconductors at absolute zero temperature by the band theory. For metals, the conduction band (top region) is partially filled, whereas, for insulators, the conduction and valence bands have a gap of 3 eV - 6 eV. In the case where there is a narrow gap between the conduction band and the valence band (about 1 eV), we call the substance a semiconductor, it becomes a weak conductor when there is electron excitation. Although the energy band picture has been very successful in classifying solids many transition metal oxides with the partially filled d band has shown to be a poor conductor and largely they are insulators (e.g., NiO, CO_2, V_2O_3).

For materials like NiO, the electron-electron interaction plays an important role: the Coulomb repulsion between electrons can be the source of their behavior as an insulator. Mott was the first to construct important approximations so that a strong correlation of electrons could lead to a insulator state. This insulator is called the Mott insulator. Mott considers a lattice consisting of a single

electron orbital per site. In the absence of electron correlation, a single band will be formed due to the overlapping of atomic orbitals in the system, the region will be filled when two electrons have opposite spins on each side. However, with two electrons that they have opposite spins there would be a Coulomb repulsion, where Mott argued that the band would split in two levels: the lower level is formed from an electron occupying an empty site, the higher region is formed formed when an electron takes the place of an existing electron. For each electron on each side the lower region is filled, the system is insulator.

The first theoretical model proposed to explain for the phase transition between metals and Mott insulator is the Hubbard model. The model is written in the second quantization formalism

$$H = -t \sum_{<ij>} \left(c_{i\sigma}^{\dagger} c_{j\sigma} + H.c. \right) + U \sum_{i} \left(n_{i\uparrow} - \frac{1}{2} \right) \left(n_{i\downarrow} - \frac{1}{2} \right) - \mu N, \tag{1.1.1}$$

with $c_{i\sigma}^{\dagger}$ ($c_{i\sigma}$) is a creation opperator (annihilation opperator) of an electron at site i with spin σ. The competition between U and t determines whether the system is in the Mott insulator phase or in the metal phase.

1.1.2 Anderson insulator

Disorder is very common in crystal solids. In fact, the lattice is never perfect, there will have impurities, defects, excess or empty atoms and lead to the breaking of translation invariance. In 1958, Anderson introduced a new view of disorder, according to which even a small amount of disorder can qualitatively and significantly affect the physical properties of the system. The metal-insulator phase transition caused by disorder is called the Anderson phase transition, the insulator is called the Anderson insulator (or Anderson localization). If $d = 1$, it can be exactly proved that the localization must happen whenever how small the disorder is. As for $d = 2$, there is no exact solution, has no phase transition and begins to have a phase transition in the dimensionality $d = 3$.

This problem can be understood within the framework of a quantum transport theory. However, its main qualitative features, among which weak and strong localization, can be captured by a multiple-scattering picture, which proves an intuitive tool to appreciate the effect of disorder. The incoming wave is assumed to propagate freely through space and to undergo elastic scattering from each impurity. Then all the waves are scattered many times interference and the wavefunction density are the result of a complex interference process. As a result, quantum interference increases

the probability of returning to the original position (contribution of the loop trajectories), although the motion is still diffuse but the diffusion constant and conductivity decrease.

When there is no disorder, the wave function of the electron in a periodic lattice is the Bloch wave function. But when there is disorder, instead of treating electrons as propagating waves with short lifetimes, they can be viewed as confined waves in space with long lifetimes. The wavefuntion $\psi(r) \approx A \exp^{-|r-r_0|/\xi}$ of electron like an exponentially funtion in space with ξ defined as localization length.

1.2 Typical Medium Theory

1.2.1 Dynamic mean field theory (DMFT)

Dynamic mean field theory is developed to approach problems involving strong correlations, based on the main idea of replacing a lattice model by a single-site quantum impurity problem embedded in an effective medium determine self-consistent. The main aim of dynamic mean field theory is that instead of dealing with lattice problems with many degrees of freedom, we consider a single-site quantum impurity embedded in a bath of non-interacting electrons containing all the remaining degrees of freedom. Then the problem will be reduced to the Anderson problem of an effective medium, the degrees of freedom of the electron bath are approximated by a hybridization function and must be determined by self-consistent equation. The local action can be represented through the free "Weiss" mean field propagator $\mathcal{G}(\tau_1 - \tau_2)$ as follows

$$S_{loc} = -\int_0^\beta d\tau_1 \int_0^\beta d\tau_2 \sum_\sigma \sum_{j,k\neq 0} c^*_\sigma(\tau_1)\mathcal{G}^{-1}_\sigma(\tau_1-\tau_2)c_{0\sigma}(\tau_2) + U\int_0^\beta d\tau c^*_\uparrow(\tau)c_\uparrow(\tau)c^*_{0\downarrow}(\tau)c_{0\downarrow}(\tau). \tag{1.2.1}$$

We have a relationship between the Green function $G^{(0)}_{ij\sigma}(\tau - \tau')$ with site $i = 0$ is removed and the full lattice Green function, i.e,

$$G^{(0)}_{ij\sigma} = G_{ij\sigma} - G_{i0\sigma}G^{-1}_{00\sigma}G_{0j\sigma}, \tag{1.2.2}$$

which holds for a general lattice. It is convenient to express the relationship between the local Green function $G_{00\sigma} \equiv G_\sigma$ and the "Weiss" mean field $\mathcal{G}^{-1}$ in the form of a Dyson equation

$$G_\sigma^{-1}(i\omega_n) = \mathcal{G}_\sigma^{-1}(i\omega_n) - \Sigma_\sigma(i\omega_n) = i\omega_n + \mu - \Delta_\sigma(i\omega_n) - \Sigma_\sigma(i\omega_n).$$

When $d \to \infty$ we have $\Sigma_\sigma(\mathbf{k}, \omega) \equiv \Sigma_\sigma(\omega)$, the lattice Green function in $\mathbf{k}$ space, $G_{\mathbf{k}\sigma}(i\omega_n)$ is given by

$$G_{\mathbf{k}\sigma}(i\omega_n) = \frac{1}{i\omega_n - \varepsilon_{\mathbf{k}} + \mu - \Sigma_\sigma(i\omega_n)}. \tag{1.2.3}$$

Performing the lattice Hilbert transform we recover the local Green function

$$G_\sigma(i\omega_n) = \sum_{\mathbf{k}\sigma} G_{\mathbf{k}\sigma}(i\omega_n) = \int_{-\infty}^{\infty} d\varepsilon \frac{\rho_0(\omega)}{i\omega_n - \varepsilon + \mu - \Sigma_\sigma(i\omega_n)},$$

with $\rho_0(\omega)$ corresponding to the non-interacting density of states. The self-consistent of DMFT equation is closed by equation

$$G_\sigma(i\omega_n) = -\frac{1}{Z} \int \prod_\sigma Dc_{0\sigma}^* Dc_{0\sigma} [c_\sigma(i\omega_n) c_{0\sigma}^*(i\omega_n)] \exp[-S_{loc}], \tag{1.2.4}$$

with $Z = \int \prod Dc_{i\sigma}^* Dc_{i\sigma} \exp[-S_{loc}]$. The equations (1.2.1)-(1.2.4) provide a closed set of equations for $G_\sigma(i\omega_n)$ and self-energy $\Sigma_\sigma(i\omega_n)$. However, the single impurity problem is still a complicate problem, which cannot, in general, be solved exactly.

1.2.2 Dynamic mean field theory (DMFT)- Typical medium theory (TMT)

DMFT can extend the problem of electronic correlation with local disorder. The Hamiltonian of AHM reads

$$\hat{H} = -t \sum_{ij,\sigma} c_{i\sigma}^\dagger c_{j\sigma} + \sum_{i\sigma} \varepsilon_i n_{i\sigma} + U \sum_i \hat{n}_{i\uparrow} \hat{n}_{i\downarrow}, \tag{1.2.5}$$

the ionic energy ε_i is a random variable follow a box probability distribution $P(\varepsilon_i)$. If within the framework of the DMFT the effect of disorder can be determined through the mean of the local density of states (LDOS), when there is no interaction ($U = 0$) the method becomes a CPA approximation, it does not describe a Anderson transition. To fix this problem Dobrosavljevic and

co-workers have proposed a variant of the DMFT where the typical value of the LDOS as an order parameter for the Anderson transition. That theory is called typical medium theory (TMT). The typical value of LDOS is approximated by the geometric average of LDOS.

The typical value of local density of states can be evaluated by

$$\rho_{\text{typ}}(\omega) = \exp\left\{\int d\varepsilon_i P(\varepsilon_i) \ln \rho(\omega, \varepsilon_i)\right\}, \tag{1.2.6}$$

with LDOS $\rho(\omega, \varepsilon_i) = -1/\pi \Im G(\omega, \varepsilon_i)$. The Green function corresponding to the $\rho_{\text{typ}}(\omega)$ is determined by the Hilbert transform

$$G_{\text{typ}} = \int_{-\infty}^{+\infty} d\omega' \frac{\rho_{\text{typ}}(\omega')}{\omega - \omega'}. \tag{1.2.7}$$

Then, The loop is closed by setting the Green function of the effective medium G_{em} equal to the local Green function, e.g.,

$$G_{\text{em}}(\omega) = G_0(\omega - \Sigma(\omega)) = G_{\text{typ}}(\omega). \tag{1.2.8}$$

here, the steps are determined by the equations (1.2.6)-(1.2.8) are not exclusive to the problem of no interaction. The same strategy can be used in any theory characterized by a local self energy.

1.3 Ultralcold atoms in optical lattice

1.3.0.1 Optical lattice

Methods for storing and trapping neutral atoms or charged particles used in experiments are the key to scientific advances, covering physics in the vast energy range from the elementary particles to the ultracold atomic quantum matter. Here, we focus on trapping neutral atoms using optical dipole trap. To form a lattice of atoms, one has to create trap potentials arranged in a periodic lattice. This can be done using coherent laser beams opposite to each other. Two beams of waves that interfere to form a standing wave with sites are fixed in space. When we introduce ultralcold atoms, the wave junctions or the wave belly are atomic confinement points depending on lattice is blue-deturned traps or red-deturned traps. If two pairs of beams are used in two perpendicular directions, then we can create a 2D lattice, if we use three pairs of beams we can create a 3D lattice.

1.3.1 Disordered optical lattice

Disorder can be introduced into the ultracold atomic systems in several ways. An efficient way to generate random potential is based on the dipole force caused by the electric field. When applied to an electric field $\mathbf{E}(\mathbf{r})$ such as a laser, atom will interaction with this field and leads to a potential called dipole potential

$$V(\mathbf{r}) = \frac{3\pi c^2 \Gamma I(r)}{2\omega_0^3 \Delta}, \tag{1.3.1}$$

where $I(r)$ is intensive of electric field, Γ is the scattering rate. Δ is the difference between the frequency of the laser beam ω_L and the oscillation eigenfrequency of atom ω_0: If $\Delta < 0$ (red-deturned dipole trap), the potential is repulsive, if $\Delta > 0$ (blue-deturned dipole trap), the potential is attractive.

Chapter 2

DISORDERED FERMIONS SYSTEMS WITH GAUSS DISTRIBUTION

2.1 Anderson Hubbard Model

2.1.1 Model and Methods

We consider the system described by the Anderson- Hubbard model

$$H = -t \sum_{<ij>\sigma} \left(a^{\dagger}_{i\sigma} a_{j\sigma} + \text{H.c.} \right) + \sum_{i} \varepsilon_i n_{i\sigma} + U \sum_{i\sigma} n_{i\uparrow} n_{i\downarrow}, \tag{2.1.1}$$

The local ionic energies ε_i is the radom variable follow a continuous probability distribution $P(\varepsilon_i)$. In our paper we consider the box (P_{Bo}) and Gaussian (P_{Ga}) distributions which are given by $P_{Bo} = \frac{1}{\Delta_{Bo}} \theta \left(\frac{\Delta_{Bo}}{2} - |\varepsilon_i| \right), P_{Ga} = \sqrt{\frac{6}{\pi \Delta^2_{Ga}}} \exp\left(-6\varepsilon_i^2 / \Delta^2_{Ga}\right)$ with θ is the Heaviside step function, Δ denotes the disorder strength. In order to be able to compare the two different distributions, the value of Δ_{Ga} is chosen such that the variance of the Gaussian distribution equal that of the box distribution $\Delta_{Bo} = \Delta_{Ga} = \Delta$.

The effective single-impurity Anderson Hamiltonian with different ε_i reads

$$H_{imp} = \sum_{\sigma} (\varepsilon_i - \mu) n_{i\sigma} + U n_{i\uparrow} n_{i\downarrow} + \sum_{k\sigma} \varepsilon_k c^{\dagger}_{k\sigma} c_{k\sigma} + \sum_{k\sigma} \left(V_k c^{\dagger}_{k\sigma} a_{i\sigma} + V^*_k a^{\dagger}_{i\sigma} c_{k\sigma} \right), \tag{2.1.2}$$

The hybridization function is related to the matrix element V_k và the dispersion parameter ε_k by

$$\eta(\omega) = \sum_k \frac{|V_k|^2}{\omega - \varepsilon_k}. \tag{2.1.3}$$

For each ionic energy ε_i, we first calculate the local density of states (LDOS) $\rho(\omega, \varepsilon_i) = -\Im G(\omega, \varepsilon_i)/\pi$. We can then obtain the geometrically averaged LDOS $\rho_{geom} = \exp\left[\langle \ln \rho(\omega, \varepsilon_i)\rangle\right]$ as well as the arithmetically averaged DOS $\rho_{arith} = \langle \rho(\omega, \varepsilon_i)\rangle$, with $\langle O(\varepsilon_i)\rangle = \int d\varepsilon_i P(\varepsilon_i) O(\varepsilon_i)$. The lattice Green function is obtained from Hilbert transformation $G_\alpha(\omega) = \int d\omega' \frac{\rho_\alpha(\omega')}{\omega - \omega'}$, with α denotes for "arith" or "geom". Here, We consider the Bethe lattice with infinite connectivity, $\rho_0(\varepsilon) = \frac{4}{\pi W}\sqrt{1 - 4(\varepsilon/W)^2}$, W is the band width, the self-consistent condition is given by $\eta(\omega) = W^2 G(\omega)/16$. We employ the equations of motion to solve impurity problem. We focus on the paramagnetic case at half-filling, for which $\langle n_\uparrow\rangle = \langle n_\downarrow\rangle = \langle n_i\rangle/2$ và $\mu = U/2$. The impurity Green function can be approximately obtained by equation

$$\begin{aligned} G(\omega, \varepsilon_i) = & \frac{1 - < n_i > /2}{\omega - \varepsilon_i + U/2 - \eta(\omega) + U\eta(\omega)[\omega - \varepsilon_i - U/2 - 3\eta(\omega)]^{-1}} \\ & + \frac{< n_i > /2}{\omega - \varepsilon_i - U/2 - \eta(\omega) - U\eta(\omega)[\omega - \varepsilon_i + U/2 - 3\eta(\omega)]^{-1}}. \end{aligned} \tag{2.1.4}$$

Next, we derive the linearized DMFT equations. The purely imaginary of Green function at the Fermi level leads to the recursive relation $G(0)^{(n+1)} = -i\pi\rho_\alpha^{(n)}$,where the left hand side in the (n + 1)th iteration step is given by the result from the (n)th iteration step. On the metallic side the LDOS is arbitrarily small in the vicinity of the MIT region, we get

$$\begin{aligned} I_{geom}(U, \Delta) = & 2 + \ln\left[3\left(\frac{U}{2}\right)^2 + \left(\frac{\Delta}{2}\right)^2\right] + \frac{2\sqrt{3}U}{\Delta}\arctan\left(\frac{\Delta}{\sqrt{3}U}\right) \\ & - 2\ln\left[\left(\frac{U}{2}\right)^2 - \left(\frac{\Delta}{2}\right)^2\right] - \frac{2U}{\Delta}\ln\frac{\Delta + U}{|\Delta - U|}, \text{ for } \Delta < U. \end{aligned} \tag{2.1.5}$$

$$\begin{aligned} I_{geom}(U, \Delta) = & -\frac{4U}{\Delta}\ln 2U + (1 + \frac{2U}{\Delta})\ln\left[\left(\frac{\Delta}{2} + \frac{U}{2}\right)^2 - \frac{U^2}{4}\right] \\ & + \frac{U}{\Delta}\ln\frac{\Delta + 3U}{\Delta + U} + \frac{\pi U}{\sqrt{3}\Delta} + 2 - 2\ln\left|\left(\frac{U}{2}\right)^2 - \left(\frac{\Delta}{2}\right)^2\right| \\ & - \frac{2U}{\Delta}\ln\frac{\Delta + U}{|\Delta - U|}, \text{ for } \Delta > U. \end{aligned} \tag{2.1.6}$$

For the linearized DMFT with arithmetical mean, the integral converges if only $\Delta < U$ for $\langle n_i \rangle = 1$ and in this case

$$I_{arith} = \frac{1}{\Delta}\left[-\frac{2x}{x^2-a^2} - \frac{1}{2a}\ln\left|\frac{x-a}{x+a}\right|\right]\Bigg|_{-\Delta/2}^{\Delta/2}$$
$$= \frac{2}{\left(\frac{U}{2}\right)^2 - \left(\frac{\Delta}{2}\right)^2} + \frac{2}{\Delta U}\ln\frac{\Delta+U}{|\Delta-U|} \tag{2.1.7}$$

Then, the equations (2.1.5), (2.1.6) and (2.1.7) are the lineared-DMFT equations of U and Δ for both averaged LDOS.

2.1.2 Results and Discussion

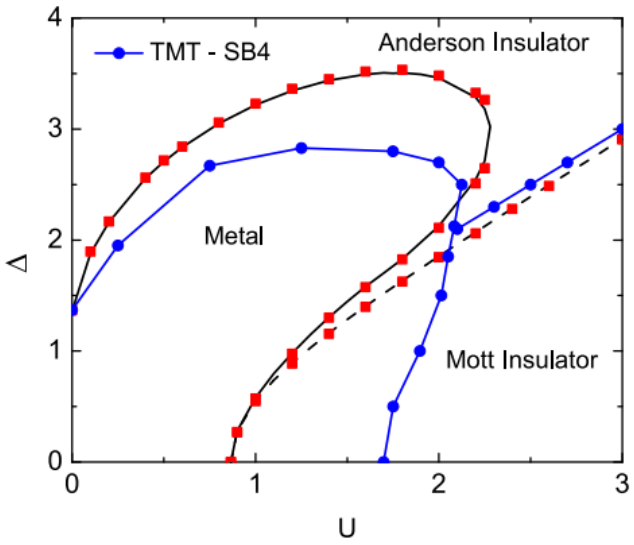

Figure 2.1.1: T = 0 phase diagram for the half filled Anderson - Hubbard model with the box disorder distribution: a comparison between TMT-DMFT with the EOM and the SB4 result in M.C.O. Aguiar, 2009 (Physical Review Letters, 102, 156402) (solid line with dots). In our result: solid (dashed) lines are determined by using geometrical (arithmetical) averaging from the linearized DMFT; squares are obtained from numerical solution of the DMFT equations. Energy parameters U, Δ are in the unit set by $W = 1$.

At $T = 0$, the interaction - disorder (U -Δ) phase diagram of the AHM with the box disorder distribution is shown in (2.1.1). We compare our result with result obtained from the numerical solution using four slave bosons to the TMT-DMFT (Physical Review Letters, 102, 156402). It is seen that the overall structure is reproduced: the two insulating phases, Mott insulator and Anderson localization, surround the correlated metal. The latter is identified for small values of U and Δ. Whereas, the Mott phase stabilizes with increasing U, and large Δ favors the Anderson

localization. Furthermore, the shape of metallic region is in good agreement and the boundary between two types of insulators occurs at $\Delta \approx U$ when $U \geq 2$. . To sum up the comparison, our result within TMT-DMFT with the EOM is justified on a qualitative level. The ground state phase diagram of the AHM with the Gaussian disorder distribution is presented in (2.1.2).There is not a big difference between the two phase diagrams shown in (2.1.1) và (2.1.2). For both disorder distributions one finds a metallic core for small and intermediate strengths of both the disorder and the interaction. We find that for small values of U the critical disorder strength in the system with the Gaussian distribution is larger than those in the system with the box distribution. For example, in the non-interacting system the critical disorder $\Delta_c(U = 0) \approx 1.66$ for the Gaussian distribution larger than those $\Delta_c(U = 0) \approx 1.36$ for the box distribution, which is in reasonable agreement with numerical results from the literature (Physical Review B, 92, 014209). From (2.1.2) one can see

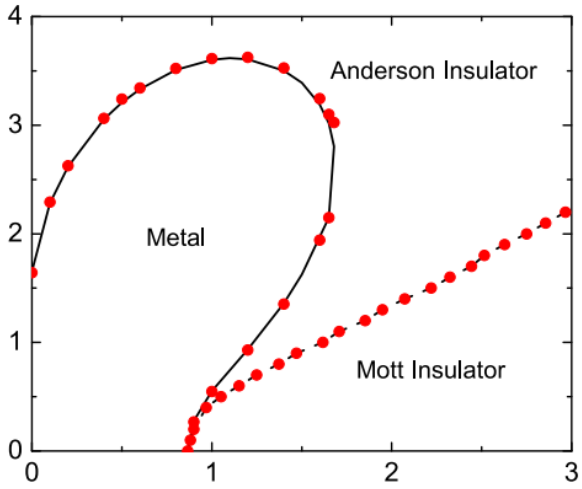

Figure 2.1.2: $T = 0$ phase diagram for the half filled Anderson - Hubbard model with the Gaussian disorder distribution, obtained from TMT-DMFT with the EOM. Solid line is determined by using geometrical averaging from the linearized DMFT; dots are obtained from numerical solution of the DMFT equations, dashed line is a guide to the eye.

that the border between the Mott and the Anderson insulators for the system with the Gaussian distribution is located lower than those with the box distribution in the (U, Δ) plane.

2.2 Anderson Falicov-Kimball model (AFKM)

2.2.1 Model and Methods

We consider the Anderson - Falicov - Kimball model, as defined by the following Hamiltonian

$$H = -\sum_{<i,j>} t_{i,j} c_i^\dagger c_j + \sum_i \varepsilon_i c_i^\dagger c_i + \sum_i U_i f_i^\dagger f_i c_i^\dagger c_i - \mu \sum_i c_i^\dagger c_i, \tag{2.2.1}$$

with $c_i^\dagger(c_i)$ and $f_i^\dagger(f_i)$ are fermionic creation (annihilation) operators for the mobile and immobile particles at a lattice site i. t_{ij} is a hopping amplitude for mobile particles between i and j, U_i the local interaction strength between mobile and immobile particles occupying in the same site i. ε_i is the local impurity. These two quantities are randomly distributed through the lattice, we assume a Gaussian distribution for impurities $P(\varepsilon_i) = \sqrt{\frac{6}{\pi\Delta^2}} \exp\left(-6\varepsilon_i^2/\Delta\right)$ and a box distribution for local Coulomb interaction $\tilde{P} = \theta(\delta/2 - |U_i - U|)/\delta$, where θ is the step function, $\Delta(\delta)$ measures the amount of Anderson (Coulomb) disorder, and U s the mean value of the Coulomb interaction strength. Here, we deal only with the repulsive interaction, $U_i \geq 0$, which leads to $U \geq \delta/2$. The mean particle number for the mobile and trapped fermions at the ith site are given by $n_i =< c_i^\dagger c_i >$ and $p_i =< f_i^\dagger f_i >$, and they are independent from each other.

The AFKM is solved within the DMFT combined with the TMT. The equation of motion for Hamiltonian (2.2.1). The local Green $G_{ii}(\omega)$ and self-energy $\Sigma_i(\omega)$ are given by, here we assume the lattice to be homogeneous with $p_i = p$ and $p \in [0, 1]$)

$$G_{ii}(\omega) = \frac{1}{\omega + \mu - \varepsilon_i - \eta(\omega) - \Sigma_i(\omega)} \equiv G(\omega, \varepsilon_i), \tag{2.2.2}$$

$$\Sigma_i(\omega) = pU_i + \frac{p(1-p)U^2}{\omega + \mu - \varepsilon_i - (1-p)U_i - \eta(\omega)}. \tag{2.2.3}$$

The local density of states is $\rho_i(\omega) = -\frac{1}{\pi}\mathrm{Im}[G_{ii}(\omega)]$. Then, the both average of LDOS are given by

$$\rho_{arith}(\omega) = \int dU_i \int d\varepsilon P(\varepsilon_i)\tilde{P}(U_i)\rho(\omega, \varepsilon_i, U_i), \tag{2.2.4}$$

$$\rho_{geom}(\omega) = \exp\left[\int dU_i \int d\varepsilon P(\varepsilon_i)\tilde{P}(U_i) \ln \rho(\omega, \varepsilon_i, U_i)\right]. \tag{2.2.5}$$

The lattice, i.e., translationally invariant, Green function is obtained by the Hilbert transform

$G_{\alpha,\mathrm{typ}}(\omega) = \int d\omega' \frac{\rho_\alpha(\omega')}{\omega - \omega'}$, with α stands for either "geom" or "arith". We consider the Bethe lattice with infinite connectivity, $\rho_0(\varepsilon) = 4\sqrt{1-4(\varepsilon/W)^2}$, for which the self-consistent condition is given by $\eta(\omega) = W^2 G(\omega)/16$. In addition, we study the band is half - filled, i.e., $\langle n_i \rangle = \langle n \rangle = 1/2$ and $p = 1/2$, $\mu = U/2$.

To proceed further, we note that in the half-filled band case, the ground state properties can be determined by the averaged LDOS at the Fermi level $\rho_{arith}(\omega)$ and $\rho_{geom}(\omega)$ at $(\omega = 0)$: (i) $\rho_{geom}(0) > 0$ denotes a metallic phase, (ii) $\rho_{arith}(0) = 0$ indicates a Mott insulator phase (hard gap). (iii) $\rho_{arith}(0) > 0$ and $\rho_{geom}(0) = 0$ denote a Anderson insulator phase (gapless). In addition, the Green function at the Fermi level is purely imaginary, $G(0) = -i\pi\rho_\alpha(0)$ and on the metallic side the LDOS is arbitrarily small in the vicinity of the MIT region. Therefore, the transition points on the phase diagram can be found by linearizing the DMFT equations. The equations which determine the MIT for both arithmetic and geometric means, respectively, take the form

$$1 = \sqrt{\frac{6}{\pi}} \frac{1}{4\Delta\delta} \int_0^\infty d\varepsilon_i \left[\frac{U/2 - \delta/4}{(U/2-\delta/4)^2 - \varepsilon_i^2} - \frac{U/2 + \delta/4}{(U/2+\delta/4)^2 - \varepsilon_i^2} \right] e^{-\frac{6\varepsilon_i^2}{\Delta^2}}, \tag{2.2.6}$$

$$1 = \frac{W^2}{16} \exp\left[\frac{4}{\Delta\delta} \sqrt{\frac{6}{\pi}} \int_0^\infty d\varepsilon_i f(\delta, U, \varepsilon_i) e^{-\frac{6\varepsilon_i^2}{\Delta^2}} \right], \tag{2.2.7}$$

with $f(\delta, U, \varepsilon_i) = t\ln[t^2+\varepsilon^2] - 2t\ln|t^2-\varepsilon^2| + 2t + 2\varepsilon\left(\arctan\frac{t}{3} + \ln\left|\frac{t-\varepsilon}{t+\varepsilon}\right|\right)\Big|_{t_1}^{t_2}$, where $t_1 = \frac{U}{2} - \frac{\delta}{4}$, $t_2 = \frac{U}{2} + \frac{\delta}{4}$.
For each value of δ the equations (2.2.6) and (2.2.7), which determined the Δ-U phase diagram.

2.2.2 Results and Discussion

Firstly, we calculate the case without Coulomb disorder ($\delta = 0$), the $U - \Delta$ phase diagram of AFKM of AFKM with the Gaussian impurity disorder distribution is shown in (2.2.1) ((dash gray lines) as well as well as in (2.2.2) (top-left part). As in the case of the box impurity disorder distribution (Physical Review B, 71, 205105), we find that the metallic phase is identified for small value of U and Δ, the Mott insulator appears when we increases U the Anderson insulator naturally overcomes for large Δ. This is clearly seen in (2.2.1) we show that the major effect of including Coulomb disorder is the narrowing of the metal and the Mott insulator regions as the strength of Coulomb disorder increases. We note that all the critical curves presented in (2.2.1) were obtained directly

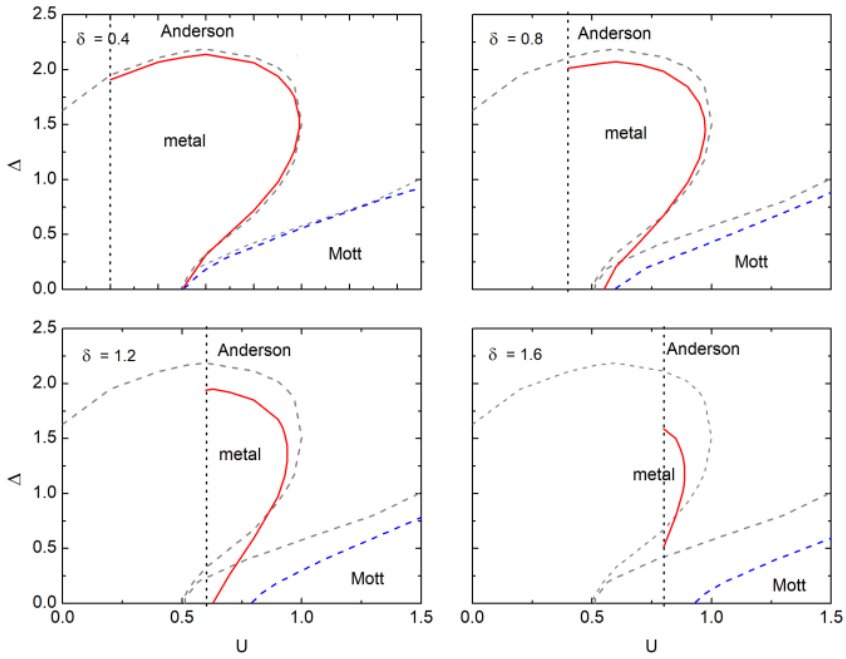

Figure 2.2.1: Phase diagrams of the AFKM for different Coulomb disorder strengths (solid red (dash blue) lines for geometric (arithmetic) mean) compared with the $\delta = 0$ case (dash gray lines). The vertical dotted line splits the regions for which $U < \delta/2$ (left side; not considered) and $U \leq \delta/2$ (right side). W sets the energy unit.

from equations (2.2.6) - (2.2.7), however, it can verified that the numerical results obtained by solving the self - consistent equations of DMFT absolutely matches with those from the linearised DMFT. In (2.2.2) we compare our result with those obtained in the European Physical Journal B, 87, 160, where the AFKM with box distribution for the local impurities $P(\varepsilon_i) = \theta(\Delta/2 - |\varepsilon_i|)/\Delta$ and box distribution for Coulomb interaction strength $\tilde{P}(U_i) = \theta(\delta/2 - |U_i + U|)$. In order to be able to compare the box and Gaussian distributions, we choose their variances equal. There is not a big difference between the two phase diagrams when $\delta = 0$: for both disorder distributions one finds a metallic core for small and intermediate strengths of both the disorder and the interaction. However, on a quantitative level the results differ each other. We find that for small values of U, the critical disorder strength in the system with the Gaussian distribution is larger than those in the system with the box distribution.

2.2.3 Conclusions

SIn summary, in this chapter we study the influence of Gauss distribution of disorder into the nonmagnetic ground state phase diagram for AFKM and AHM using the equation of motion as an

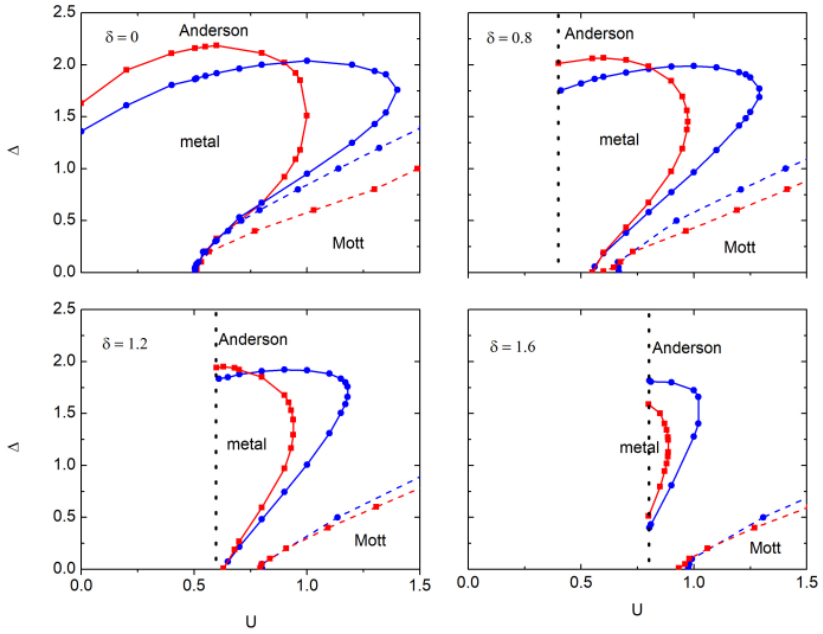

Figure 2.2.2: Phase diagrams of the AFKM with the Gaussian impurity disorder distribution and the box Coulomb disorder distribution (our result, red lines with squares) compared to those with the box impurity distribution and the box Coulomb disorder distribution in The European Physical Journal B, 87, 160 (blue lines with dots).

impurity solver. We show that within DMFT-TMT the phase diagrams of the AFKM and AHM with the Gaussian distribution for impurities are qualitatively similar. For AFKM, We show that the metallic and Mott insulator regimes shrink as the local Coulomb disordered strengths increases.

Chapter 3

ASYMMETRIC ANDERSON HUBBARD MODEL AND ANDERSON HUBBARD MODEL WITH SITE-DEPENDENT INTERACTIONS

3.1 Asymetric Anderson Hubbard Model (Mass imbalance)

3.1.1 Model and Methods

The Hamiltonian model is solved within the DMFT. The effective single impurity Anderson model with different ε_i reads

$$H_{imp} = \sum_{\sigma}(\varepsilon_i - \mu_\alpha)n_{i\sigma} + Un_{i\uparrow}n_{i\downarrow} + \sum_{k\sigma}\varepsilon_{k\sigma}c^{\dagger}_{k\sigma}c_{k\sigma} + \sum_{k\sigma}\left(V_{k\sigma}c^{\dagger}_{k\sigma}a_{i\sigma} + V^{*}_{k\sigma}a^{\dagger}_{i\sigma}c_{k\sigma}\right), \tag{3.1.1}$$

SWe now employ the equations of motion method (3.1.1) for solving the effective single impurity Anderson model, The local Green function in this case can be approximately expressed as (2.1.4)

$$G_\sigma(\omega,\varepsilon_i) = \frac{1- < n_i > /2}{\omega-\varepsilon_i+U/2-\eta_\sigma(\omega)+U\eta_{\bar\sigma}(\omega)[\omega-\varepsilon_i-U/2-\eta_\sigma(\omega)-2\eta_{\bar\sigma}(\omega)]^{-1}} + \frac{< n_i > /2}{\omega-\varepsilon_i-U/2-\eta_\sigma(\omega)-U\eta_{\bar\sigma}(\omega)[\omega-\varepsilon_i-+U/2-\eta_\sigma(\omega)-2\eta_{\bar\sigma}(\omega)]^{-1}}, \tag{3.1.2}$$

where $\eta_\sigma(\omega) = t_\sigma^2 G_\sigma(\omega)$. Equation (3.1.2) reproduces the result (in Physical Review B, 71, 205105) for $r = 0$ and in the mass imbalance AHM $r = 1$ ($t_\uparrow = t_\downarrow$) in Hoang 2019 (Physica B: Condensed Matter, 570, 320-323). In the non-disorder case $\varepsilon_i = 0$, equation 3.1.2 is reduced to the mass-imbalance HM case in Hoang 2016 (Journal of the Korean Physical Society, 68, 238-242) and I. V. Stasyuk 2005 (The European Physical Jounal B, 48, 339-348)..

The linearized DMFT equations determining the MIT for both geometrical and arithmetical mean can be obtained for $\rho_{\uparrow\alpha}$ and $\rho_{\downarrow\alpha}$, α denotes $a(g)$ corresponding to "arith" and "geom". The A pair of linear equations for

$$[I_1(U,\Delta)-1][r^2 I_1(U\Delta-1)] - [UI_2(U,\Delta)r]^2 = 0 \tag{3.1.3}$$

with $t_{\uparrow\alpha} = 1$ sets the energy unit, $t_{\downarrow\alpha} = r$.

$$I_1(U,\Delta) = \frac{1}{\Delta}\int_{-\Delta/2}^{\Delta/2} d\varepsilon \frac{\varepsilon^2 + U^2/4 + (1-n_i)U\varepsilon}{[\varepsilon^2 - U^2/4]^2}, \tag{3.1.4}$$

$$I_2(U,\Delta) = \frac{1}{\Delta}\int_{-\Delta/2}^{\Delta/2} d\varepsilon \frac{U/2 + (1-n_i)\varepsilon}{[\varepsilon^2 - U^2/4]^2}. \tag{3.1.5}$$

In the two limits $r = 0$ and $r = 1$ equation (3.1.3) is reduced to equation (15) in Byczuk 2005 (Physical Review B, 71, 205105) and equation (11) in Hoang 2019 (Physica B: Condensed Matter, 570, 320-323), correspondingly.

The equations for $\rho_{\uparrow g}(0)$ and $\rho_{\downarrow g(0)}$ are also obtained

$$\rho_{\uparrow g}(0) = \exp\left[\frac{1}{\Delta}\int_{-\Delta/2}^{\Delta/2} \ln\left(\frac{t_{\uparrow}^2\left[\varepsilon^2 + U^2/4 + (1-n_i)U\varepsilon\right]\rho_{\uparrow g}(0)}{[\varepsilon^2 - U^2/4]^2} + \frac{Ut_{\downarrow}^2\left[U/2 + (1-n_i)\varepsilon\right]\rho_{\downarrow g}(0)}{[\varepsilon^2 - U^2/4]^2}\right) d\varepsilon\right] \tag{3.1.6}$$

$$\rho_{\downarrow g}(0) = \exp\left[\frac{1}{\Delta}\int_{-\Delta/2}^{\Delta/2} \ln\left(\frac{Ut_{\downarrow}^2\left[U/2 + (1-n_i)\varepsilon\right]\rho_{\uparrow g}(0)}{[\varepsilon^2 - U^2/4]^2} + \frac{t_{\uparrow}^2\left[\varepsilon^2 + U^2/4 + (1-n_i)U\varepsilon\right]\rho_{\downarrow g}(0)}{[\varepsilon^2 - U^2/4]^2}\right) d\varepsilon\right]. \tag{3.1.7}$$

3.1.2 Results and Discussion

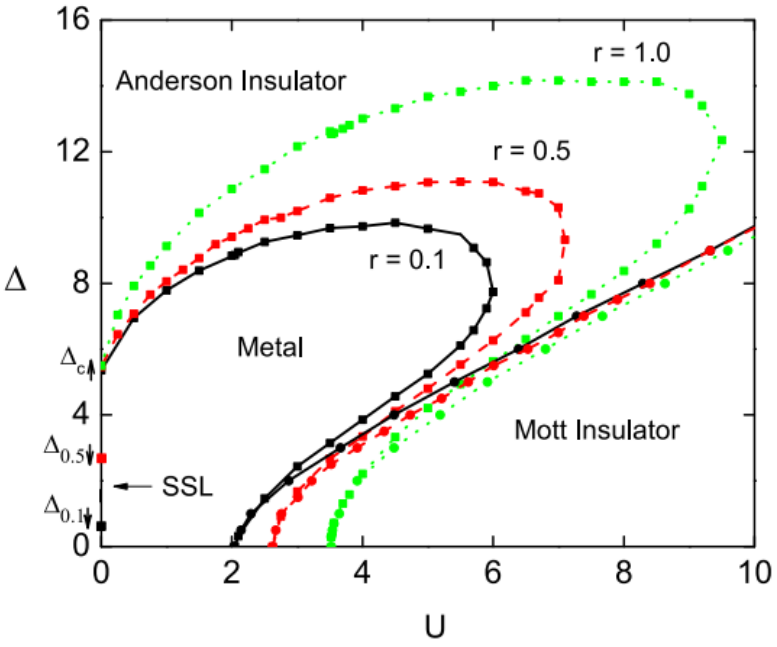

Figure 3.1.1: (Color online) Nonmagnetic ground state phase diagram for the half-filled AHM with mass imbalance for different values of $r = 0.1, 0.5$ and comparison with the result of the balanced case $r = 1$. Solid with squares (solid with dots) lines are determined by using geometrical (arithmetical) averaging for $r = 0.1$. Dash with squares (dash with dots) lines are determined by using geometrical (arithmetical) averaging for $r = 0.5$. Dot with squares (dot with dots) lines are determined by using geometrical (arithmetical) averaging for the balanced case $r = 1$. The spin-selective localized phase is located in the line $U = 0, \Delta_{r\downarrow} < \Delta < \Delta_{c\downarrow}$.

KThe main result of our investigation is the nonmagnetic ground state phase diagram of the mass imbalanced AHM at half-filling shown in (3.1.1) for $r = 0.1, 0.5, 1.0$. For $0 < r < 1$ four different phases are observed in the phase diagram: (1)The Anderson insulator phase is defined by $\rho_{\sigma g}(0) = 0, \rho_{\sigma a}(0) > 0$. In the non-interacting system ($U = 0$), the critical disorder strength

$\Delta_{c\uparrow}(U=0)=2e$ for all r. Similar to the mass balanced case, here, larger Δ favors the Anderson localization. In addition, the Anderson insulator region is enlarged with increasing the mass imbalance (r decreases) because at fixed $t_\uparrow$, the larger the difference in the bare mass, the smaller $t_\downarrow$ and the easier it is to localize the system. (2) The Mott insulator phase is identified by $\rho_{\sigma a}(0)=0$. As in the balanced case the Mott insulator stabilizes with increasing U. Furthermore, its region is enlarged with increasing the mass imbalance (r decreases) for the same reason as the Anderson insulator. (3) The metal is determined by $\rho_{\sigma g}(0)>0$ and found for small values of U and Δ. Its shape is similar to those of the balanced case, but its region is reduced with increasing the mass imbalance (r decreases) because the region of both types of insulator are enlarged. (4) The partially localized or spin-selective localized phase, where the spin-down particles are localized ($\rho_{\downarrow g}(0)=0$) while those with spin-up are still itinerant ($\rho_{\uparrow g}(0)>0$). PThis phase originates from the mass imbalance in the system and takes place when $U=0$ và $2er=\Delta_{r\downarrow}(U=0)<\Delta<\Delta_{c\uparrow}(U=0)=2e$. It should be noted that without interaction ($U=0$) the two spin components are independent, and the spinselective localized phase can be found, but as soon as the interaction is switched ($U\neq 0$) on the two spin components are coupled, as a result $\rho_{\uparrow g}(0)$ and $\rho_{\downarrow g}(0)$ are vanished simultaneously and the spin-selective localized phase no longer exists.

3.2 Anderson Hubbard Model with site-dependent interactions

3.2.1 Model and methods

The Hamiltonian of AHM reads

$$H=-t\sum_{<i,j>,\sigma}(a^{\dagger}_{i\sigma}a_{j\sigma}+\text{h.c.})+\sum_{i\sigma}(\varepsilon_i-\mu_\sigma)n_{i\sigma}+U\sum_i\left[n_{i\uparrow}n_{i\downarrow}-\frac{1}{2}\left(n_{i\uparrow}+n_{i\downarrow}\right)\right], \tag{3.2.1}$$

where ε_i follow a box probability distribution with Δ denotes the Anderson disorder strength.In our paper we consider two types of site-dependent Coulomb repulsion U_i:

(i) U_i is assumed as random and uniformly distributed within the interval $[U-\delta/2;U+\delta/2]$, U is the mean value of the on-site interaction, δ is the Coulomb disorder strength. Here, we only consider the repulsive interaction, $U_i\geq 0$, from which $U\geq\delta/2$.

(ii) $U_i$is spatially alternating interactions in a bipartite lattice, i.e., $U_i=U_s$ in the sublattice $s=A,B$.

Within the DMFT, Hamiltonian (3.2.1) is mapped onto an effective Anderson model as follows

$$H_{imp} = \sum_{\sigma}(\varepsilon_i - \mu)n_{i\sigma} + U_i\left[n_{i\uparrow}n_{i\downarrow} - \frac{1}{2}\left(n_{i\uparrow} + n_{i\downarrow}\right)\right] + \sum_{k,\sigma}\varepsilon_k c^{\dagger}_{k\sigma}c_{k\sigma} + \sum_{k\sigma}\left(V_k c^{\dagger}_{k\sigma}a_{i\sigma} + V^{*}_{k}a^{\dagger}_{i\sigma}c_{k\sigma}\right). \tag{3.2.2}$$

We restrict our study to the nonmagnetic case at half-filling, for which $\langle n_{i\uparrow}\rangle = \langle n_{i\downarrow}\rangle = \langle n_i\rangle/2$ và $\mu = 0$. By decoupling the equations of motion at second order, the impurity Green function can be approximated as follow

$$G_{\sigma}(\omega,\varepsilon_i) = \frac{1- < n_i > /2}{\omega - \varepsilon_i + U_i/2 - \eta_i(\omega) + U_i\eta_i(\omega)[\omega - \varepsilon_i - U_i/2 - 3\eta_i(\omega)]^{-1}} + \frac{< n_i > /2}{\omega - \varepsilon_i - U_i/2 - \eta_{\sigma}(\omega) - U_i\eta_{\bar{\sigma}}(\omega)[\omega - \varepsilon_i - +U/2 - \eta_{\sigma}(\omega) - 2\eta_{\bar{\sigma}}(\omega)]^{-1}}, \tag{3.2.3}$$

where $\eta_i(\omega)$ is the hybridization function, which describes the coupling of lattice site i with all other sites of the system within the DMFT. Here $U_i = U_s, \eta_i = \eta_s$ if $i \in s$-sublattice for the case of spatially alternating interactions, while η_i is site-independent for the case of random interactions. In the non-disorder limits $\varepsilon_i = 0$, $U_i = U$, equation (3.2.3) is the recovery of the (full) Hubbard III approximation of the Hubbard model at half-filling.

(i) *Random on-site interactions.* The arithmetic and geometric mean of the LDOS can be evaluated by

$$\rho_{arith}(\omega) = \int dU_i \int d\varepsilon P(\varepsilon)\tilde{P}(U_i)\rho(\omega,\varepsilon_i,U_i), \tag{3.2.4}$$

$$\rho_{geom}(\omega) = \exp\left[\int dU_i \int d\varepsilon P(\varepsilon)\tilde{P}(U_i)\ln\rho(\omega,\varepsilon_i,U_i)\right]. \tag{3.2.5}$$

The linearized DMFT equations with arithmetic and geometric means, which determine the boundary curves between metallic and insulating phases, are obtained as

$$1 = \frac{W^2}{16\Delta\delta}\int dU_i \int d\varepsilon Y(\varepsilon,U_i), \tag{3.2.6}$$

$$1 = \frac{W^2}{16}\exp\left[\frac{1}{\Delta\delta}\int dU_i \int d\varepsilon \ln Y(\varepsilon,U_i)\right], \tag{3.2.7}$$

where $Y(\varepsilon,U_i) = \dfrac{\varepsilon^2 + 3U_i^2/4 + 2\varepsilon U_i(1-\langle n_i\rangle)}{[\varepsilon^2 - U^2/4]^2}$.

(ii) *Spatially alternating interactions.* The arithmetically and geometrically averaged LDOS for

s-sublattice can be now is given by

$$\rho_{s,arith}(\omega) = \int d\varepsilon P(\varepsilon)\rho(\omega,\varepsilon,U_s), \tag{3.2.8}$$

$$\rho_{s,geom}(\omega) = \exp\left[\int d\varepsilon P(\varepsilon)\ln\rho(\omega,\varepsilon_i,U_s)\right]. \tag{3.2.9}$$

The Green function for s-sublattice is obtained by corresponding Hilbert transform. Similary, we also obtain the equations of linearized DMFT as follow

$$1 = \frac{W^2}{16}\exp\left[I_{geom}(U_A,U_B,\Delta)\right], \tag{3.2.10}$$

where $I_{geom}(U_A,U_B,\Delta) = \dfrac{1}{2\Delta}\int d\varepsilon_i \ln\left[Y_A(\varepsilon_i)Y_B(\varepsilon_i)\right]$, for the linearized DMFT with geometric mean, and

$$1 = \frac{W^2}{16} I_{arith}(U_A,U_B,\Delta), \tag{3.2.11}$$

where $I_{arith}(U_A,U_B,\Delta) = \frac{1}{\Delta}\left[\int d\varepsilon_i Y_A(\varepsilon_i)\int d\varepsilon Y_B(\varepsilon_i)\right]^{1/2}$, for the linearized DMFT with arithmetic mean, $Y_s(\varepsilon_i) = \dfrac{\varepsilon_i^2 + 3U_s^2/4 + 2\varepsilon_i U_s(1-\langle n_i\rangle)}{[\varepsilon_i^2 - U_s^2/4]^2}$.

3.2.2 Results and discussion

The ground state will be investigated from the obtained values of ρ_{arith} and ρ_{geom} : (1) $\rho_{arith}(0) \neq 0$ and $\rho_{geom}(0) \neq 0$ indicate a metallic phase, (2) $\rho_{arith}(0) = 0$, $\rho_{geom}(0) = 0$ and $\int \rho_{geom}(\omega)d\omega \neq 0$ give a Mott insulating phase, (3) $\int \rho_{geom}(\omega)d\omega = 0$ specifies an Anderson localized phase, (4) $\rho_{arith}(0) \neq 0$, $\rho_{geom}(0) = 0$ and $\int \rho_{geom}(\omega)d\omega \neq 0$ specify localized states inside the Mott gap

(i) *Random on-site interactions.* Figure (3.2.1) depics the $U-\Delta$ nonmagnetic phase diagrams of the half-filled AHM for various Coulomb disorder strengths. The system can be in a metallic phase, a MI, localized states inside the Mott gap or an Anderson localization phase. It should be noted that the metallic domain and the Mott insulating domain are only connected when $\delta = 0$. In the presence of Coulomb disorder, $\delta \neq 0$,one can see that the metallic domain and the Mott insulating domain is separated by the localized states inside the Mott gap. The extended states (metallic region) and the true band gap are no longer connected as the localized states are in between. If the Coulomb disorder increases, the metallic and Mott insulating regions shrink, whereas the Anderson localized region is enlarged. When the Coulomb disorder reaches its maximum, $\delta = 2U$, the Mott insulating

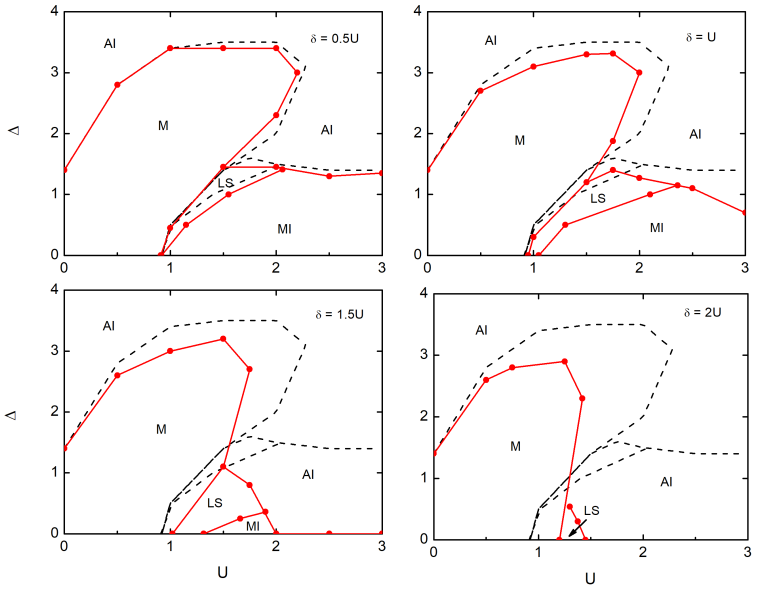

Figure 3.2.1: Phase diagram of the half-filled AHM for different Coulomb disorder strengths (solid line) compared with the $\delta = 0$ case (dash lines). M, AI, MI and LS stand for metal, AI, MI and localized states in the Mott gap, respectively. Energy scale: $W = 1$.

region disappears, and the system enters either a metallic, Anderson localized phase or localized states inside the Mott gap. When $\delta = 2U$, the Coulomb strength U_i at a given site will range from 0 to $2U$; thus, when taking the arithmetic average, there will always be a distribution from non-interacting electrons ($U_i = 0$) that prevents the establishment of a Mott insulating phase. Both Anderson disorder and Coulomb disorder support Anderson localization and prevent the metallic phase as well as the MI from being established. But only Coulomb disorder can suppress the Mott insulating completely. In addition to the narrowing of the metallic and MI regions, the presence of Coulomb disorder gives rise to a new region where the system is in a localized state.

(ii)*Spatially alternating interactions.* In order to present our numerical results for spatially alternating interactions, we set $U_B = U$ and $r = U_B/U_A$ and r: $0 < r < 1$. The nonmagnetic groundstate phase diagram, the main result of our investigation for spatially alternating interactions, is shown in figure 6 for different values of r = 0.5, 0.8 and 1.0. In this phase diagram we do not distinguish the Mott insulating phase from localized states inside the Mott gap one, but simply refer them to a disordered MI. For $0 < r < 1$ three different phases (metal, MI and AI) can be seen in the phase diagram as $r = 1$, but the metallic region is reduced, and the AI region is enlarged by decreasing the spatial modulation parameter e.

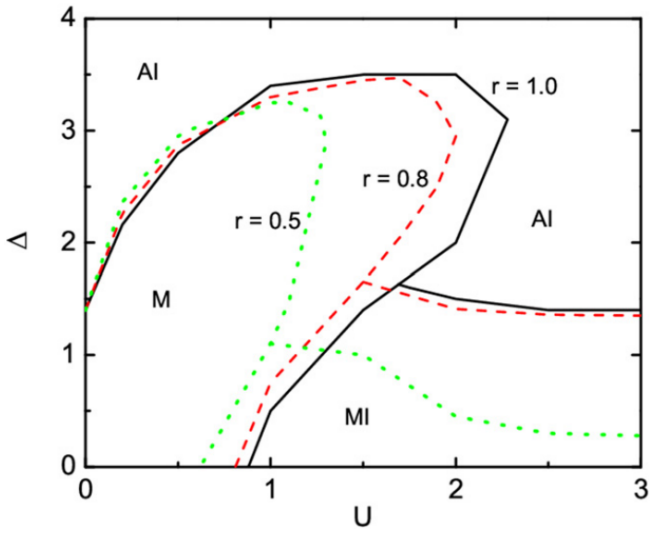

Figure 3.2.2: Phase diagram of the half-filled AHM with spatially alternating interactions for different values of $r = 0.5, 0.8$ compared with $r = 1$. M, AI and MI stand for metal, AI, and disordered MI, respectively

3.2.3 Conclusions

In the mass-imbalance AHM case, in addition to the three phases showed up in the balanced case, the phase diagram of the mass imbalanced case contains a spin-selective localized phase, where one spin component is metallic while the other spin component is insulating.

In the AHM with site-dependent interactions case, we figure out that the presence of Coulomb disorder drives the system toward the Anderson localized phase that can occur even in the absence of Anderson structural disorder. For the spatially alternating interactions, we find that the metallic region is reduced and the Anderson insulator one is enlarged with increasing interaction modulation.

CONCLUSIONS

In this thesis, we want to investigate the influence of disorder and correlation in two models AHM and AFKM through four problems in chapter 2 and chapter 3. (1)-(2) Investigate the influence of Gaussian distribution on the phase diagram of two models AHM and AFKM. The similar overall form of the phase diagram as well as the averaged local densities of states obtained from the box and Gaussian disorder distribution indicate that qualitatively they are not dependent on the choice of the above disorder distributions. However, note that this conclusion is derived within the TMT - DMFT with an approximation to the equation of motion as an impurity solver. (3) We have studied the ground state phase diagram of the mass imbalanced AHM at half-filling. In addition to the three phases that showed up in the balanced case, the phase diagram of the mass imbalanced case contains a spin-selective localized phase. For $0 < r < 1$ we found that excluding the non-interacting case the phase transition occurs simultaneously for two spin components, both the Anderson and Mott insulator region are enlarged and the metallic one is reduced as the mass imbalance increased. The phase diagram of the mass imbalanced AHM also differs from those of the balanced case by the fact that the spin-selective localized phase is appeared in the line $U = 0$, $\Delta_{r\downarrow} < \Delta < \Delta_{c\uparrow}$. (4) we studied the solutions of the half-filled AHM with site-dependent local interactions. The two simplest types of site-dependent interactions considered in the presence paper are the random and uniformly distributed one and the spatially alternating one in the lattice. In the case of random and uniformly distributed interactions, we showed that Coulomb disorder has the main effect of driving the system from a metallic state to the Anderson localized phase, and the Anderson localized states appear even in the absence of Anderson structural disorder. For the spatially alternating interactions, we find that the metallic region is reduced and the Anderson insulator one is enlarged with increasing interaction modulation.

Publications

1. A. T. Hoang, T. H. Y. Nguyen, D. A. Le, 2019, Metal-insulator phase diagram of the half-filled Anderson - Hubbard model, *Physica B: Condensed Matter*, 570, 320-323.

2. T. H. Y. Nguyen, A. T. Hoang, 2021, Phase diagram of the half-filled Anderson- Falicov-Kimball model with Coulomb disorder, *Journal of Physics: Conference Series*, 1932, 012013.

3. A. T. Hoang, T. H. Y. Nguyen, D. A. Le, 2021, Metal–insulator transitions of fermionic mixtures with mass imbalance in disordered optical lattice, *Modern Physics Letters B*, 35, 2150357.

4. T. H. Y. Nguyen, D. A. Le and A. T. Hoang, 2022, Anderson localization in the Anderson - Hubbard model with site-dependent interactions, *New Journal of Physics*, 24, 053054.

5. T. H. Y. Nguyen, A. T. Hoang, D. A. Le, 2022, Influence of Coulomb disorder on the phase diagrams of the Anderson - Hubbard model, *Journal of Physics: Conference Series*, 2269, 012004.